Environmental Science & Technology

Article

pubs.acs.org/est

# Mechanism of the Selective Catalytic Oxidation of Slip Ammonia over Ru-Modified Ce−Zr Complexes Determined by in Situ Diffuse Reflectance Infrared Fourier Transform Spectroscopy

Wanmiao Chen, Yongpeng Ma, Zan Qu,* Qinghang Liu, Wenjun Huang, Xiaofang Hu, and Naiqiang Yan*

School of Environmental Science and Engineering, Shanghai Jiao Tong University, Shanghai 200240, China

Supporting Information

**ABSTRACT:** The slip ammonia from selective catalytic reduction (SCR) of $NO_x$ in coal-fired flue gas can result in deterioration of the utilities or even the environmental issues. To achieve selective catalytic oxidation (SCO) of slip ammonia, Ru-modified Ce−Zr solid solution catalysts were prepared and evaluated under various conditions. It was found that the Ru/$Ce_{0.6}Zr_{0.4}O_2$(polyvinylpyrrolidone (PVP)) catalyst displayed significant catalytic activity and the slip ammonia was almost completely removed with the coexistence of $NO_x$ and $SO_2$. Interestingly, the effect of $SO_2$ on $NH_3$ oxidation was bifacial, and the $N_2$ selectivity of the resulting products was as high as 100% in the presence of $SO_2$ and $NH_3$. The mechanism of the SCO of $NH_3$ over Ru/$Ce_{0.6}Zr_{0.4}O_2$(PVP) was studied using various techniques, and the results showed that $NH_3$ oxidation follows an internal SCR (iSCR) mechanism. The adsorbed ammonia was first activated and reacted with lattice oxygen atoms to form an −HNO intermediate. Then, the −HNO mainly reacted with atomic oxygen from $O_2$ to form NO. Meanwhile, the formed NO interacted with $-NH_2$ to $N_2$ with $N_2O$ as the byproduct, but the presence of $SO_2$ can effectively inhibit the production of $N_2O$.

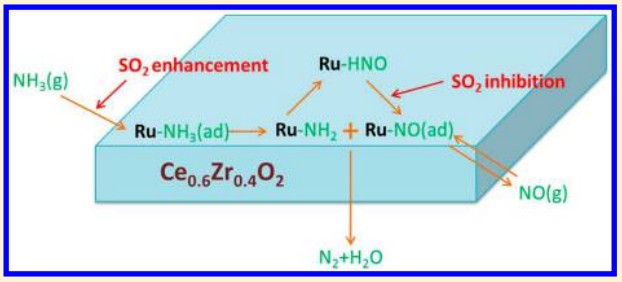


## INTRODUCTION

As major air pollutants, nitrogen oxides ($NO_x$), which contribute to photochemical smog, acid rain, ozone depletion, and greenhouse effects, are mainly generated from the combustion of fossil fuels from mobile and stationary pollution sources.[1] Selective catalytic reduction (SCR) of $NO_x$ with $NH_3$ is a mature technology for reducing $NO_x$ emission from coal-fired power plants. However, the unreacted ammonia slip from SCR units, especially for aged catalysts, has always drawn wide attention. Because slip ammonia can cause a dust plug in the downstream air-preheater and form secondary inorganic aerosols that contribute significantly to $PM_{2.5}$ after it is released into the atmosphere, it has been regarded as a more sensitive air pollutant than $NO_x$.[2] Therefore, the allowable slip ammonia concentration of SCR units in coal-fired power plants has been tentatively regulated to less than 3 ppm in China.[3] Meanwhile, the mercury emitted from coal-fired power plants is also a worldwide concern, especially for China as the largest mercury emitting country.[4] An international treaty regarding mercury pollution (the Minamata Convention on Mercury) was officially signed in October, 2013,[5] and it is a significant challenge for China to reduce excessive mercury emission because of the high consumption of coal.[6,7] Simultaneously removing the slip ammonia and elemental mercury using one multiple-effect catalyst has been proposed for installation at the tail-end of SCR units in our previous research.[8]

In our previous research, we found that employing Ru as the dopant to modify SCR catalysts can significantly enhance the oxidation of elemental mercury and the mechanism was discussed accordingly.[9] However, the selective catalytic oxidation (SCO) of $NH_3$ to $N_2$ over Ru catalysts has rarely been involved. Ru has been used as a catalyst for high concentration $NH_3$ synthesis and decomposition,[10] which indicates that Ru has the potential to be a promising active component for $NH_3$−SCO. Recently, ceria(Ce)−zirconia(Zr) solid solutions with cubic fluorite phases (Ce−Zr > 1:1) have served as catalyst carriers in many studies and drawn more attention due to their outstanding oxygen storage capacities and unique redox properties.[11] Moreover, Ce−Zr solid solution supported metal oxide catalysts exhibited excellent catalytic activity and $N_2$ selectivity for NO reduction via $NH_3$.[12] Although the pathways of $NH_3$−SCO and $NH_3$−SCR are not identical, Ce−Zr solid solutions could be an attractive catalyst support for $NH_3$−SCO.

Since the catalytic oxidation activity and mechanism of mercury oxidation over Ru-modified catalysts has already been studied in detail,[9] the SCO of $NH_3$ over Ru catalysts was the main focus of this study. Ru/$Ce_xZr_{1-x}O_2$ was used as the

Received: May 13, 2014
Revised: August 30, 2014
Accepted: September 17, 2014
Published: September 17, 2014





dx.doi.org/10.1021/es502369f | Environ. Sci. Technol. 2014, 48, 12199−12205

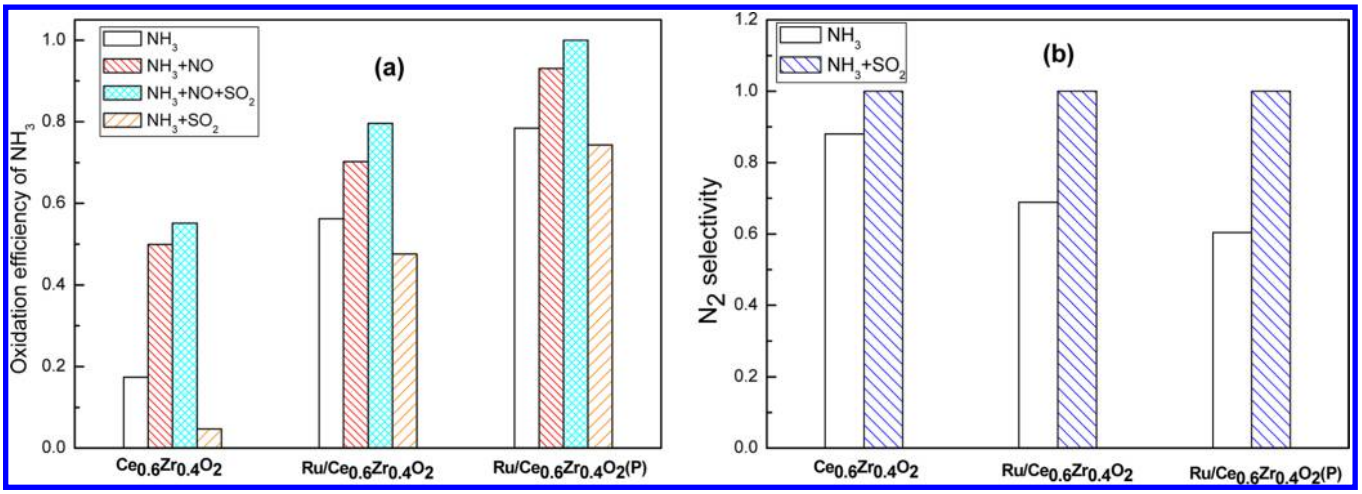


**Figure 1.** (a) The $NH_3$−SCO efficiencies over various catalysts at 350 °C. (b) $N_2$ selectivity of $NH_3$−SCO with or without $SO_2$ over various catalysts at 350 °C. Space velocity (SV) was approximately $3 \times 10^5$ $h^{-1}$. The temperature was 623 K. Thirty ppm of $NH_3$, 30 ppm of NO, and 500 ppm of $SO_2$. The other gas compositions were 4% $O_2$ and $N_2$.

multiple-effect catalyst, and polyvinylpyrrolidone (PVP) was employed to enhance the dispersion of the low concentration Ru. The $NH_3$ oxidation activity and $N_2$ selectivity over different catalysts at various conditions was tested. Although several studies have examined the $NH_3$−SCO process, the mechanism of $NH_3$ oxidation and $N_2$ formation is not clearly understood. Three major reaction pathways have been proposed for the SCO of $NH_3$ to $N_2$ over different catalysts.[13,14] However, the mechanism of $NH_3$−SCO over Ru doping catalysts has not been studied in detail. To rationally develop the process of $NH_3$ oxidation to $N_2$ over Ru-modified catalysts, the reaction mechanism must be clarified. Temperature-programmed oxidation (TPO), temperature-programmed desorption (TPD), and in situ diffuse reflectance infrared Fourier transform spectroscopy (DRIFT) were used to determine the possible reaction mechanisms.

## EXPERIMENTAL SECTION

**Materials and Catalyst Preparation.** The Ru doping catalysts were synthesized according to a literature method.[15] Polyvinylpyrrolidone (PVP, Mw = 58 000) and quantitative $RuCl_3 \cdot xH_2O$ was dissolved in 30 mL of ethanol. The mixture was refluxed at 100 °C for 3 h. Next, an Ru colloidal solution was added to $Ce_xZr_{1-x}O_2$ (Supporting Information), and the mixture was dried at 60 °C with electromagnetic stirring. Then, the catalysts were calcined at 400 °C for 5 h in air with a 1 °C/min ramping rate from room temperature and labeled as Ru/$Ce_xZr_{1-x}O_2$(PVP). The Ru/$Ce_xZ_{1-x}O_2$ catalysts were prepared using the normal wet impregnation method. The Ru oxide content of $Ce_xZr_{1-x}O_2$ was set at 0.2 wt % for all catalysts. All chemicals used for the preparation of catalysts were of analytical grade and were purchased from Sigma-Aldrich Co. or Sinopharm Chemical Reagent Co. The $SO_2$, $NH_3$, and $NO_x$ gases were supplied by Dalian Date Gas Co.

**Catalytic Activity Measurement.** The performances of the catalysts for $NH_3$ oxidation were tested in a fixed-bed quartz reactor. The catalyst particles were placed in the reactor with quartz wool under atmospheric pressure and were heated using a vertical electrical furnace. The feed gases consisting of 30 ppm of $NO_x$, 30 ppm of $NH_3$, 4% $O_2$, and 500 ppm of $SO_2$ in $N_2$ were adjusted by mass flow controllers and introduced into the reactor at a total flow rate of 500 sccm. The concentrations of $NH_3$, NO, $NO_2$, and $N_2O$ were continually monitored with FTIR Multigas analyzer (IMACC, E-3200-C). The $NH_3$-TPO was performed from 50 to 400 °C with a 1 °C/min ramping rate. The $NH_3$ removal efficiency and $N_2$ selectivity were calculated using eqs 1 and 2:

$$\text{NH}_3 \text{ removal efficiency} = \frac{[\text{NH}_3]_{\text{inlet}} - [\text{NH}_3]_{\text{outlet}}}{[\text{NH}_3]_{\text{inlet}}} \times 100\% \quad (1)$$

$$\text{N}_2 \text{ selectivity} = \left[1 - \frac{[\text{NO}]_{\text{outlet}} + [\text{NO}_2]_{\text{outlet}} + 2[\text{N}_2\text{O}]_{\text{outlet}}}{[\text{NH}_3]_{\text{inlet}} - [\text{NH}_3]_{\text{outlet}}}\right] \times 100\% \quad (2)$$

**$NH_3$-TPD.** The $NH_3$-TPD curves were collected using a chemisorption analyzer (2920, AutoChem II, Micromeritics). Prior to the measurement, the samples were first treated in a He stream at 350 °C to remove any physically adsorbed matter. The $NH_3$ adsorption was then performed at 100 °C with 10% $NH_3$ for 1 h. Next, the samples were purged in a He stream for 30 min to remove physically adsorbed $NH_3$ and then heated to 600 °C with a temperature ramp of 10 °C/min with a 50 sccm He flow. Desorbed $NH_3$ was detected with a thermal conductivity detector (TCD).

**In Situ DRIFT Studies.** In situ DRIFT spectra were recorded on a Fourier transform infrared spectrometer (FTIR, Nicolet 6700) equipped with a smart collector and an MCT detector cooled by liquid $N_2$. The diffuse reflectance FTIR measurements were carried out in a high-temperature cell with KCl windows. Mass flow controllers and a sample temperature controller were used to simulate the real reaction conditions. Prior to each experiment, the catalyst was heated to 400 °C in $N_2$ with a total flow rate of 250 sccm for 3 h. The IR spectra were recorded by accumulating 100 scans at a resolution of 4 $cm^{-1}$.

## RESULT AND DISCUSSION

**Catalytic Activity.** The catalytic oxidation efficiencies of the modified Ru/$Ce_{0.6}Zr_{0.4}O_2$ and Ru/$Ce_{0.6}Zr_{0.4}O_2$ (PVP) were tested and evaluated under various conditions as shown in Figure 1 (preliminary experiments showed the $Ce_{0.6}Zr_{0.4}O_2$ supported catalysts displayed superior catalytic activity). The $NH_3$ oxidation over $Ce_{0.6}Zr_{0.4}O_2$ was tested, and the efficiency is only approximately 17%. The $NH_3$ oxidation efficiency over

$Ru/Ce_{0.6}Zr_{0.4}O_2$ increased to 56%, which indicates that doping with Ru could facilitate $NH_3$ oxidation. Meanwhile, the synthetic method could also have an effect on the catalytic activity. The $NH_3$ oxidation efficiency over $Ru/Ce_{0.6}Zr_{0.4}O_2$(PVP) increases to approximately 80%. This result is ascribed to PVP, which could promote Ru dispersion over the carrier and enhance the catalytic activities in a way similar to other studies.[15] In addition, the $NH_3$ oxidation products over various catalysts were also determined. The main detectable products were NO and $N_2O$ in the absence of $NO_x$. $N_2O$ concentrations lower than 0.2 ppm were formed when 30 ppm of $NH_3$ was decomposed. However, the $N_2$ selectivity is only approximately 69% for $Ru/Ce_{0.6}Zr_{0.4}O_2$. In addition, more NO was generated during the process of $NH_3$ oxidation over PVP promoted $Ru/Ce_{0.6}Zr_{0.4}O_2$ catalysts, and the $N_2$ selectivity is approximately 10% lower than normal $Ru/Ce_{0.6}Zr_{0.4}O_2$.

$NH_3$-TPO experiments were also performed separately over three catalysts to evaluate the $NH_3$ oxidation activities (Figure S1, Supporting Information). $NH_3$ could not be oxidized, and no products were formed until the temperature was above 300 °C over $Ce_{0.6}Zr_{0.4}O_2$, while the initial temperature was approximately 250 °C over the $Ru/Ce_{0.6}Zr_{0.4}O_2$ catalyst. However, the doping of Ru in $Ce_{0.6}Zr_{0.4}O_2$ has a negative effect on the $N_2$ selectivity of products because significant amounts of NO were formed at higher temperatures (350−400 °C) over both $Ru/Ce_{0.6}Zr_{0.4}O_2$ and $Ru/Ce_{0.6}Zr_{0.4}O_2$(PVP). According to some literature reports, $NH_3$ could be oxidized at lower temperatures (<140 °C) over some catalysts (especially Ag-modified catalysts), and $N_2O$ was the main product.[13] Two disparate reaction pathways, for high and low temperatures, respectively, were proposed to explain this situation. Similar phenomena were not observed over the $Ru/Ce_{0.6}Zr_{0.4}O_2$ catalyst, which indicates that there might be only one mechanism for $NH_3$−SCO in our research.

Since the catalysts are proposed to be installed at the tail of SCR unit, $NO_x$ would exist in the flue gas during operation. Therefore, the $NH_3$ oxidation efficiencies in the presence of $NO_x$ over various catalysts were also evaluated and shown in Figure 1. As predicted, the $NH_3$ oxidation was remarkably enhanced by $NO_x$ for all catalysts. Under the test conditions, the oxidation efficiencies of $NH_3$ were approximately 70% and 93% over the $Ru/Ce_{0.6}Zr_{0.4}O_2$ and $Ru/Ce_{0.6}Zr_{0.4}O_2$(PVP) catalysts, respectively. The mechanism could be explained as $NH_3$ being oxidized through the SCR pathway in the presence of $NO_x$ (reactions 3 and 4), which indicates that the catalysts also have the potential for De-$NO_x$.

$$4NH_3 + 6NO \rightarrow 5N_2 + 6H_2O \quad (3)$$

$$8NH_3 + 6NO_2 \rightarrow 7N_2 + 12H_2O \quad (4)$$

The effect of $SO_2$ on $NH_3$ oxidation is very interesting. In the presence of $NO_x$, $SO_2$ could slightly promote the $NH_3$ oxidation efficiencies for all catalysts (Figure 1). The $NH_3$ removal efficiency over $Ru/Ce_{0.6}Zr_{0.4}$(PVP) was as high as 100% in the presence of 30 ppm of $NO_x$ and 500 ppm of $SO_2$. However, the opposite effect occurred when only $NH_3$ and $SO_2$ existed in the gas. In comparison with the situation with only ammonia, $SO_2$ negatively affected the $NH_3$ oxidation for all catalysts. In addition, the $N_2$ selectivity increased significantly to 100% because no $NO_x$ was detected during the experiment in the presence of $SO_2$ and $NH_3$ (Figure 1b). Therefore, the effect of $SO_2$ on $NH_3$ oxidation was bifacial. $SO_2$ could facilitate the $NH_3$−SCO with the coexistence of $NO_x$ and inhibited the $NH_3$−SCO in the absence of $NO_x$ with a 100% $N_2$ selectivity.

**$NH_3$-TPD.** The profiles of the $NH_3$-TPD analysis of various catalysts are given in Figure S2, Supporting Information. One major desorption peak was observed with the $Ce_{0.6}Zr_{0.4}O_2$ catalyst at 200 °C, which might be attributed to ammonia weakly adsorbed on acid sites including Lewis and Brønsted acids. After doping with Ru, the main peak at 200 °C was much weaker, and a board shoulder starting at 300 °C was observed over $Ru/Ce_{0.6}Zr_{0.4}O_2$, which indicated that the doping of Ru would bate the adsorption ability of $NH_3$. Although less $NH_3$ was adsorbed to $Ru/Ce_{0.6}Zr_{0.4}O_2$ catalyst, it displayed a better $NH_3$ oxidation efficiency because of the excellent catalytic activity of Ru. In addition, the PVP promoted $Ru/Ce_{0.6}Zr_{0.4}O_2$ displayed superior $NH_3$ adsorption capacity than that of $Ru/Ce_{0.6}Zr_{0.4}O_2$, which resulted in even better $NH_3$ catalytic oxidation activity, as shown in Figure 1. The profile of the sulfated catalyst was very different. Two major $NH_3$ desorption peaks were observed at approximately 350 and 500 °C. Less $NH_3$ desorbed from the sulfated catalyst at lower temperatures (<250 °C) than at higher temperatures, which indicated that sulfation by $SO_2$ could reinforce the bonding between $NH_3$ and the catalysts and enhance the $NH_3$ adsorption at higher temperatures. This behavior could explain the effects of $SO_2$ on $NH_3$−SCO observed in Figure 1 (discussed later).

**DRIFT of $NH_3$ Adsorption.** DRIFT spectra of the absorbed species due to contact with $NH_3$ over $Ru/Ce_{0.6}Zr_{0.4}O_2$ at different temperatures are showed in Figure 2. As shown the in figure, several bands at 1163, 1217, 1321, 1432, 1666, and 1847 $cm^{-1}$ were observed after the sample was treated with $NH_3$ at 50 °C. The bands at 1163,[16] 1432,[17] and 1666[18] $cm^{-1}$ could be assigned to asymmetric and symmetric bending vibrations of $NH_4^+$ species on Brønsted sites, while the band at 1217 $cm^{-1}$ was attributed to asymmetric and symmetric bending vibrations of the N−H bonds in $NH_3$ coordinately linked to Lewis acid sites.[19,20] In the NH stretching region, bands were found at 3246, 3348, and 3690 $cm^{-1}$, together with negative bands at 3662 and 3639 $cm^{-1}$ due to the hydroxyl consumption through interaction with $NH_3$ to form $NH_4^+$.[13] Moreover, some other bands also showed up at 1065, 1321, and 1847 $cm^{-1}$, which belonged to neither Lewis nor Brønsted acid sites. Accordingly, the band at 1065 $cm^{-1}$ might be caused by ammonia hydrogen

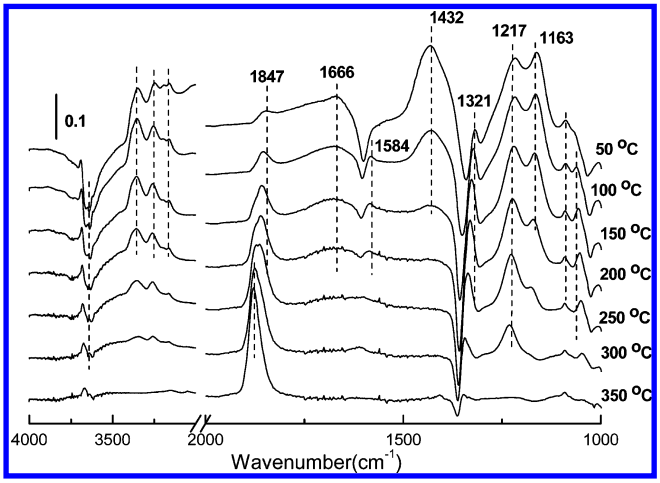


**Figure 2.** DRIFT spectra of $Ru/Ce_{0.6}Zr_{0.4}O_2$ treated with 500 ppm of $NH_3$ at 50 °C and successive purging with $N_2$ at various temperatures.


dx.doi.org/10.1021/es502369f | Environ. Sci. Technol. 2014, 48, 12199−12205

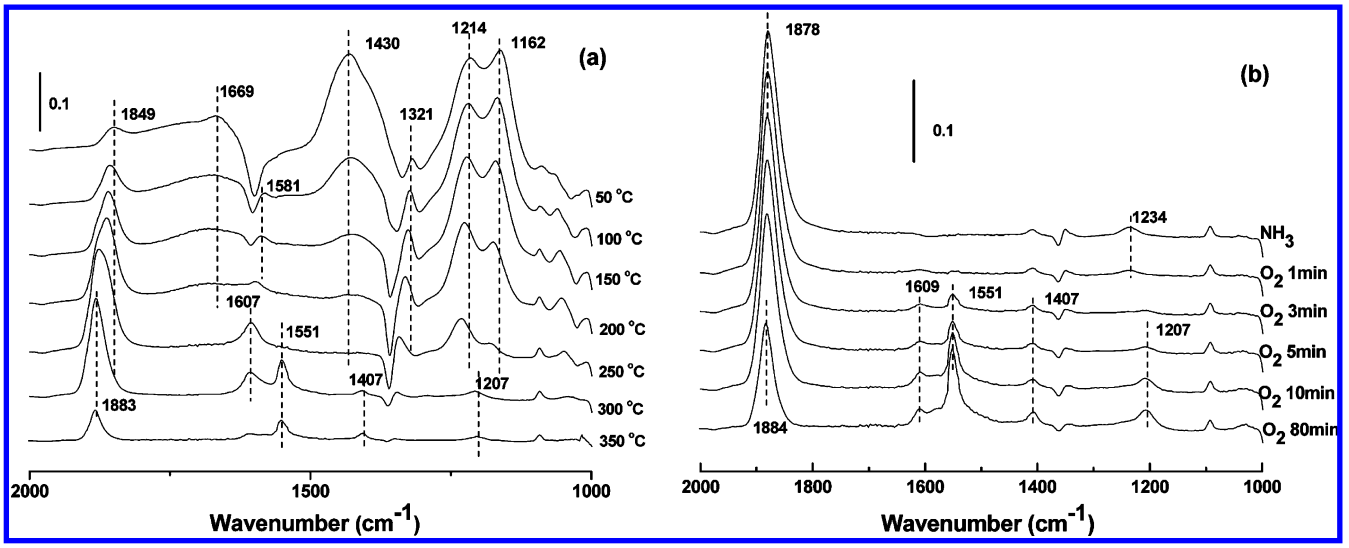


**Figure 3.** DRIFT spectra of $Ru/Ce_{0.6}Zr_{0.4}O_2$(PVP): (a) treated with 500 ppm of $NH_3$ at 50 °C and successive purging with 4% $O_2$ at various temperature; (b) interaction of $O_2$ with the $NH_3$ formed in situ at 300 °C.

bonding to the surface oxygen atoms of cerium oxide.[21] The band at 1321 $cm^{-1}$ could be due to the wagging mode of an amide species ($-NH_2$).[22] The intensities of the 1430 and 1666 $cm^{-1}$ bands assigned to Brønsted acid sites decreased noticeably at higher temperatures and vanished at 150 °C. In addition, the intensity of the band at 1164 $cm^{-1}$ was also weakened as the temperature increased and disappeared at 300 °C. The band at 1217 $cm^{-1}$, due to Lewis acid sites, still remained at 300 °C. This result indicated that ammonia bonded to Lewis acid sites were more stable.

A new peak centered at 1584 $cm^{-1}$ appeared at 100 °C, which corresponded to the $-NH_2$ species, an intermediate of the ammonia oxidation.[23] As the temperature increased, the intensities of the bands at 1321 and 1847 $cm^{-1}$ enhanced and shifted following the decrease in the bands assigned to $NH_3$. The band at 1847 $cm^{-1}$ shifted to 1870 $cm^{-1}$ at 350 °C. The band at 1870 $cm^{-1}$ was assigned to nitrosyl ($-HNO$) on Ru sites (discussed later). These results indicated that, upon heating, the adsorbed $NH_3$ could be activated to form $-NH_2$ intermediates through the abstraction of hydrogen. Accordingly, $-NH$ would be formed from the continuous dehydrogenation as the temperature increased.[13] However, no obvious band assigned to $-NH$ was observed, perhaps because the $-NH$ reacted quickly with oxygen atoms from the Ce−Zr solid solution, which has an outstanding oxygen storage capacity.

$$NH_3 \rightarrow NH_2 + H \quad (5)$$

$$NH_2 \rightarrow NH + H \quad (6)$$

$$NH + O \rightarrow HNO \quad (7)$$

**Interaction of $NH_3$ with $O_2$.** The mechanism of $NH_3$ oxidation was studied on the basis of the behavior of adsorbed $NH_3$ species interacting with $O_2$ over $Ru/Ce_{0.6}Zr_{0.4}O_2$(PVP) using in situ DRIFT(Figure 3). The bands of $NH_3$ assigned to Brønsted acid sites (1163, 1430, and 1669 $cm^{-1}$) and Lewis acid sites (1214 $cm^{-1}$) decreased gradually and disappeared at temperatures above 200 °C. When the intensities of these bands decreased, the band at 1321 $cm^{-1}$, assigned to $-NH_2$, increased from 50 to 200 °C, which agrees with the results in Figure 2. Another very weak peak at 1581 $cm^{-1}$ appeared at 100 °C and disappeared at 250 °C. Some research proposed that the band was attributed to bidentate nitrate.[24,25] However, we think that the explanation is not applicable to this situation because no $NO_x$ was generated at low temperatures, as shown in the TPO results. It is more reasonable to suggest that the band at 1581 $cm^{-1}$ is also due to amide ($-NH_2$) scissoring.[13] A new peak at 1606 $cm^{-1}$ appeared, which was attributed to bridging nitrate(nitrate species),[22] and the band of $-NH_2$ at 1342 $cm^{-1}$ decreased as the temperature increased to 250 °C. This result indicated that the adsorbed ammonia started to be oxidized with $O_2$ at temperatures of approximately 250 °C over the $Ru/Ce_{0.6}Zr_{0.4}O_2$(PVP) catalyst, which was in agreement with the TPO results. As the temperature increased to 300 °C, two new peaks at 1550 and 1208 $cm^{-1}$ showed up, and they were assigned to adsorbed nitrate species.[26,27] Upon heating to 350 °C, the intensities of all of the bands decreased due to the desorption of the produced/adsorbed NO species at higher temperatures.

In situ DRIFT spectra of $O_2$ passing over an $NH_3$-pretreated catalyst at 300 °C were also recorded and are shown in Figure 3b. After the catalyst was treated with 500 ppm of $NH_3$ and purged with $N_2$, some adsorbed ammonia species desorbed under $N_2$ purging and only a main band at 1878 $cm^{-1}$ remained and was observed. As shown in Figure 3b, the bands attributable to the produced nitrate species (1606, 1550, 1208 $cm^{-1}$) were observed after 4% $O_2$ was introduced for 3 min, which indicated that the $NH_3$ ad-species could be oxidized by $O_2$ quickly. The band at 1878 $cm^{-1}$ weakened gradually and shifted to 1884 $cm^{-1}$ after exposing the catalyst to $O_2$. The shifting of the band at 1878 $cm^{-1}$ was also observed in Figures 2 and 3a and will be discussed in detail in the following section.

**Interaction of $NH_3$ with in Situ Formed NO.** To evaluate the reaction mechanism, the interaction of $NH_3$ with the NO species formed in situ was investigated as follows: first, adsorbed NO was formed on the catalyst by exposure to NO and $O_2$ at 300 °C. Then, the sample was purged with $N_2$ for 30 min. After that, 200 ppm of $NH_3$ was introduced and in situ DRIFT spectra were recorded. The results are shown in Figure 4. Some bands assigned to nitrate ad-species at 1610, 1551, and 1206 $cm^{-1}$ were observed after the NO and $O_2$ passed over the catalysts for a brief time. Following $NH_3$ inflow for 3 min, the nitrate bands started to decrease, indicating that $NH_3$ could

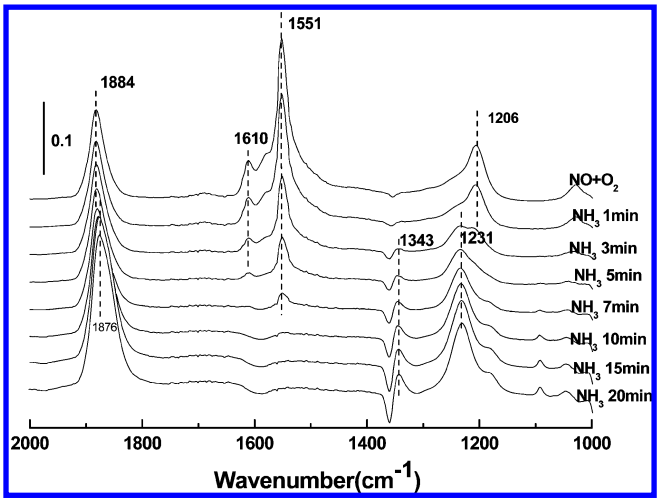


**Figure 4.** DRIFT spectra of the interaction between $NH_3$ (200 ppm) and the NO formed in situ on the $Ru/Ce_{0.6}Zr_{0.4}O_2$(PVP) catalyst at 300 °C.

quickly react with the NO species. The bands assignable to adsorbed $NH_3$ species (1343 and 1231 $cm^{-1}$) appeared on the catalyst following the $NH_3$ flow, and the intensities increased with the exposure time.

The band at 1884 $cm^{-1}$ shifted to 1876 $cm^{-1}$ following the $NH_3$ inflow. A similar shifting of the band also occurred in experiments shown in Figures 2 and 3. Accordingly, some studies proposed that the bands around 1870 $cm^{-1}$ may be related to the produced/adsorbed NO.[23] However, this is not applicable for all situations in our research, since similar bands appeared at low temperatures during $NH_3$ adsorption, shown in Figures 2 and 3, while no $NO_x$ existed according to the TPO results. According to some literature reports, the band at 1870 $cm^{-1}$ was in the typical range of coordinated nitrosyl ligands and indicated the formation of $[Ru(NH_3)_5(NO)]^{3+}$.[28] To identify the band, first, the spectra of $NH_3$ and NO adsorption over $Ce_{0.6}Zr_{0.4}O_2$ were recorded, and no identical peak appeared on the surface of $Ce_{0.6}Zr_{0.4}O_2$ in both $NH_3$ and NO DRIFT adsorption spectra (Figure S3, Supporting Information). Clearly, it can be concluded that the bands in the range of 1900 to 1800 $cm^{-1}$ are due to the Ru species in the catalysts. When the $NH_3$ passed over the NO presorbed catalyst, the band gradually shifted from 1878 to 1884 $cm^{-1}$. The shifting reversed from 1884 to 1878 $cm^{-1}$ when the $NH_3$ pretreated catalyst was exposed to NO. Similar results were also observed at 350 °C (Figures S4 and S5, Supporting Information). Therefore, it is reasonable to assign the band at 1878 $cm^{-1}$ to nitrosyl formed from the dehydrogenation of $NH_3$ adsorbed to Ru, and 1884 $cm^{-1}$ is assigned to adsorbed NO linked to Ru.

The results mentioned above clearly indicate that the oxidation of $NH_3$ over the $Ru/Ce_{0.6}Zr_{0.4}O_2$(PVP) catalyst follows an internal SCR (iSCR) mechanism, which involves the oxidation of $NH_3$ into NO species (reactions 5−9), along with adsorbed NO species interacting with amide and being reduced to $N_2$ with $N_2O$ as byproduct (reactions 10−12). The $-NH_2$ and NO species formed in situ are the intermediates in this reaction pathway. The overall reaction for SCO-$NH_3$ is reaction 13.

$$O_2 \rightarrow 2O \quad (8)$$

$$HNO + O \rightarrow NO + OH \quad (9)$$

$$NH_2 + NO \rightarrow N_2 + H_2O \quad (10)$$

$$NH + NO \rightarrow N_2O + H \quad (11)$$

$$H + OH \rightarrow H_2O \quad (12)$$

$$4NH_3 + 3O_2 \rightarrow 2N_2 + 6H_2O \quad (13)$$

**DRIFT of $SO_2$ Adsorption.** Because the results in Figure 1 showed that the effect of $SO_2$ on $NH_3$−SCO was very special, the mechanism of the $SO_2$ effect was investigated. The DRIFT spectra of the uptake of 1000 ppm of $SO_2 + O_2$ on $Ru/Ce_{0.6}O_{0.4}O_2$(PVP) at 350 °C was recorded and shown in Figure S6, Supporting Information. After exposure of $SO_2 + O_2$ for 60 min, several bands at 1970, 1630, 1387, 1191, 1052, and 979 $cm^{-1}$ were detected on the catalyst. The band at 1387 $cm^{-1}$ was attributed to the asymmetric vibration mode of O═S═O, which was a typical "organic" sulfate species with covalent S═O double bonds.[29] The bands at 1052 and 979 $cm^{-1}$ were

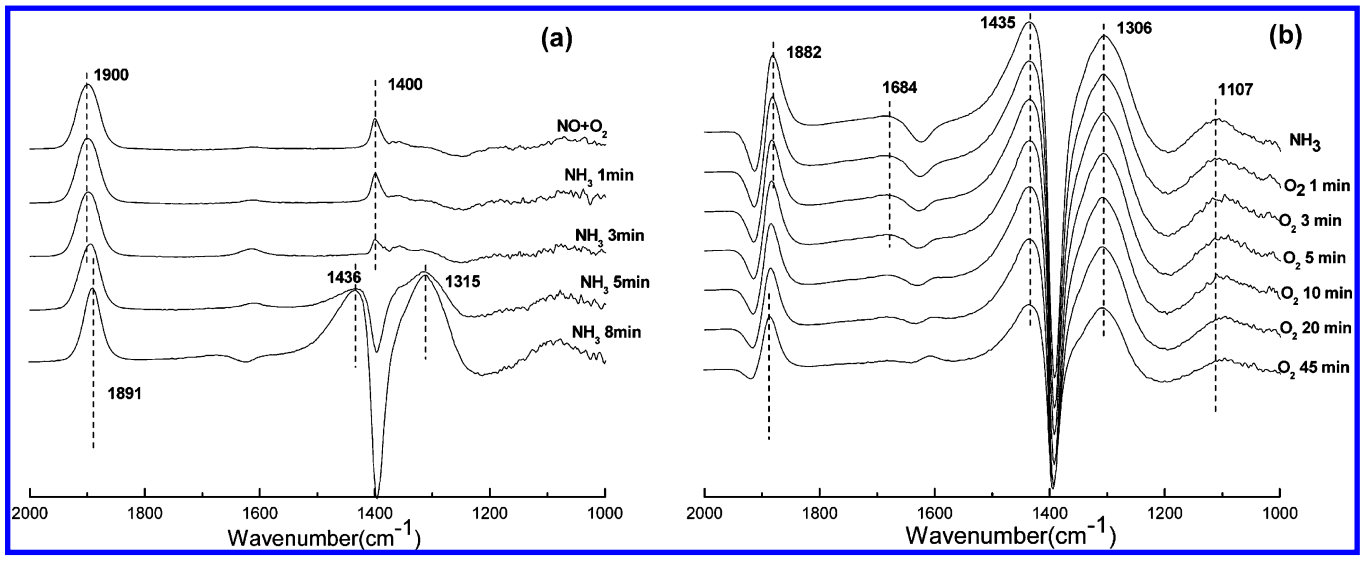


**Figure 5.** DRIFT spectra of interaction of (a) $NH_3$ (200 ppm) with the NO formed in situ and (b) 4% $O_2$ with the $NH_3$ formed in situ on sulfated $Ru/Ce_{0.6}Zr_{0.4}O_2$(PVP) catalyst at 300 °C.

assignable to the stretching motion of adsorbed sulfate on the surface, which were the triply degenerate asymmetric stretching $\nu 3$ band of the bidentate sulfate complex and nondegenerate symmetric stretching $\nu 1$ band, respectively.[30] Additionally, the strongest band at 1191 $cm^{-1}$ was attributed to bulk sulfate species.[22] The negative peak at 3656 $cm^{-1}$ was associated with the vibration of the hydroxyl groups. The consumption of surface OH species indicated an interaction between $SO_2$ and surface hydroxyl groups. It is reasonable to infer that surface water was formed because the band at 1630 $cm^{-1}$ assigned to $\delta_{HOH}$ of $H_2O$ and a broadband in the range of 3500−3100 $cm^{-1}$ in the spectra appeared synchronously.[22] The band at 1970 $cm^{-1}$ was ascribed to sulfate species linked to Ru because no identical band was detected on the sulfated $Ce_{0.6}Zr_{0.4}O_2$ catalyst (Figure S7, Supporting Information).

**DRIFT Studies of the Interaction between $NH_3$ and NO on Sulfated Catalysts.** Sulfated Ru/$Ce_{0.6}Zr_{0.4}O_2$(PVP) was first pretreated with NO + $O_2$, and then, $NH_3$ was passed over the catalyst. After the adsorption of NO + $O_2$ on the sulfated catalyst at 300 °C, bands at 1400 and 1900 $cm^{-1}$ were observed on the surface of the catalyst (Figure 5a). After the $NH_3$ passed over the sulfated Ru/$Ce_{0.6}Zr_{0.4}O_2$(PVP) catalyst, the intensity of the band at 1400 $cm^{-1}$ assigned to adsorbed NO decreased immediately. In addition, after interacting for 5 min, the band assigned to NO vanished and new bands at 1435 and 1315 $cm^{-1}$, ascribed to adsorbed $NH_3$ species, appeared. Additionally, the peak at 1900 $cm^{-1}$, assigned to NO adsorbed to Ru, shifted to 1891 $cm^{-1}$. This peak is assignable to nitrosyl linked to Ru sites, just as that in fresh Ru/$Ce_{0.6}Zr_{0.4}O_2$(PVP). This result means that the adsorbed/formed NO could still react with $NH_3$ on the sulfated catalyst through reactions 10 and 11.

The interaction of $O_2$ with adsorbed $NH_3$ was also performed over sulfated Ru/$Ce_{0.6}Zr_{0.4}O_2$(PVP), and the results are shown in Figure 5b. Bands at 1882, 1684, 1435, 1306, and 1107 $cm^{-1}$ appeared on the sulfated Ru/$Ce_{0.6}Zr_{0.4}O_2$(PVP) surface. Compared to the fresh catalyst, $NH_3$ seemed more readily adsorbed on sulfated Ru/$Ce_{0.6}Zr_{0.4}O_2$(PVP). The result was the same with $NH_3$-TPD: sulfation could enhance the adsorption of ammonia over the catalysts at high temperatures. After passing 4% $O_2$ over the $NH_3$ presorbed sulfated catalyst, the intensities of the bands assigned to the $NH_3$ species decreased very slowly. In addition, after the uptake of $O_2$ for 45 min, no obvious bands assigned to adsorbed NO species were detected on the catalysts. It is concluded that the oxidation of $-NH_2$ to NO was severely suppressed on sulfated Ru/$Ce_{0.6}Zr_{0.4}O_2$(PVP).

**Effect of $SO_2$ on the Reaction Mechanism.** It was proposed in the previous section that the $NH_3$−SCO follows the iSCR mechanism (Figure 6). When $SO_2$ was present and the catalysts were sulfated, more gaseous ammonia was adsorbed on the catalyst, which was due to the increase of the acid sites. Then, more $-NH_2$ would be generated on the surface of the catalyst as the concentration of adsorbed $NH_3$ increased. While reactions 10 and 11 were barely restricted by $SO_2$, as shown in the DRIFT result, the reactions 10 and 11 would be promoted in the presence of gaseous NO due to the formation of more $-NH_2$ on the catalyst surface. Therefore, the consumption of gaseous $NH_3$ will increase, which could explain the result shown in Figure 1: the removal efficiencies of $NH_3$ increased with the coexistence of $SO_2$ and NO.

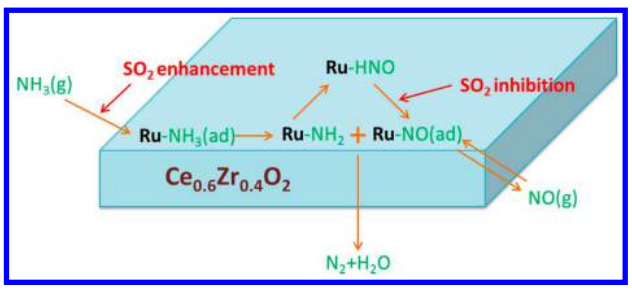


**Figure 6.** Mechanism of SCO-$NH_3$ and the effect of $SO_2$.

The situation would be different in the absence of NO. As inferred from the DRIFT result shown in Figure 5, reaction 9 was severely inhibited over the sulfated catalyst. Therefore, the $NH_3$ oxidation efficiencies over sulfated catalysts were lower than those over fresh catalysts in the absence of $NO_x$ because there are fewer intermediates: NO was formed. In the meantime, the concentration of $-NH_2$ increased as stated above. Therefore, the consumption of generated NO over the sulfated catalyst will be much quicker than over a fresh catalyst, since reactions 10 and 11 are promoted over sulfated catalysts. Because less NO was generated and consumed completely at once, none of the formed NO could desorb from the catalyst surface, which explains the result that no $NO_x$ was detected and the $N_2$ selectivity was as high as 100% with only $NH_3$ and $SO_2$. This study employed simulated flue gas streams to test the catalysts. Actually, coal-derived flue gas is a complex mixture also containing fly ash particles, carbon monoxide, and many acid gases.[31] There can be potential impacts of other acid gases such as HCl and $SO_3$ upon the catalysts for $NH_3$ oxidation,[32,33] and the deactivation of the catalysts over time could be a fruitful area for future studies and research.

In conclusion, the PVP promoted 0.2% Ru-modified $Ce_{0.6}Zr_{0.4}O_2$ catalyst displayed excellent performance for the selective catalytic oxidation of slip ammonia under various conditions. $SO_2$ can enhance the removal of slip ammonia in the presence of $NO_x$ but also slightly restrains $NH_3$ oxidation and significantly improves the $N_2$ selectivity to 100% in the absence of $NO_x$. The pathway of slip ammonia oxidation over the Ru/$Ce_{0.6}Zr_{0.4}O_2$ catalyst follows the iSCR mechanism. That is, the adsorbed ammonia is first activated and reacts with lattice oxygen atoms to form the −HNO intermediate. Then, the −HNO mainly reacts with atomic oxygen from $O_2$ to form adsorbed NO species. Finally, the resulting NO interacts with $-NH_2$ to $N_2$ with $N_2O$ as a byproduct.

## ■ ASSOCIATED CONTENT

### Ⓢ Supporting Information

Preparation of Ce-Zr solid solution; $NH_3$ temperature-programed oxidation profiles; $NH_3$ temperature-programed desorption profiles; DRIFT spectra. This material is available free of charge via the Internet at http://pubs.acs.org/.

## ■ AUTHOR INFORMATION

### Corresponding Authors

*(Z.Q.) Tel:+86 21 54745591; fax: +86 21 54745591; e-mail: quzan@sjtu.edu.cn.

*(N.Y.) Tel: +86 21 54745591; fax: +86 21 54745591; e-mail: nqyan@sjtu.edu.cn.

### Notes

The authors declare no competing financial interest.

## ■ ACKNOWLEDGMENTS

This study was supported by the National Basic Research Program of China (973) under Grant No. 2013CB430005, the NSFC projects (21077073, 21277088) and the National High-Tech R&D Program (863) of China (No. 2013AA065403).

## ■ REFERENCES

(1) Bare, J. TRACI 2.0: The tool for the reduction and assessment of chemical and other environmental impacts 2.0. *Clean Technol. Environ. Policy* **2011**, *13* (5), 687−696.

(2) Ward, T.; Trost, B.; Conner, J.; Flanagan, J.; Jayanty, R. Source apportionment of PM2.5 in a subarctic airshed-fairbanks, Alaska. *Aerosol Air Qual. Res.* **2012**, *12* (4), 536−543.

(3) Ministry of the Environmental Protection, The People's Republic of China. *Engineering technical specification of flue gas selective catalytic reduction denitrification for thermal power plant*; HJ 562−2010; MEP: Beijing, 2010.

(4) Wang, H. Y.; Ma, Z. H.; Lu, P. S.; Cao, Y.; Pan, W. P. Modeling of Mercury Speciation and Capture in Coal-Fired Flue Gas. In *Cleaner Combustion and Sustainable World*; Springer: Berlin, 2013; pp 515−519.

(5) McNutt, M. Mercury and health. *Science* **2013**, *341* (6153), 1430−1430.

(6) Cheng, C. M.; Cao, Y.; Kai, Z.; Pan, W. P. Co-effects of sulfur dioxide load and oxidation air on mercury re-emission in forced-oxidation limestone flue gas desulfurization wet scrubber. *Fuel* **2013**, *106*, 505−511.

(7) Li, X.; Liu, Z. Y.; Kim, J.; Lee, J. Y. Heterogeneous catalytic reaction of elemental mercury vapor over cupric chloride for mercury emissions control. *Appl. Catal., B: Environ.* **2013**, *132*, 401−407.

(8) Chen, W. M.; Ma, Y. P.; Yan, N. Q.; Qu, Z.; Yang, S. J.; Xie, J. K.; Guo, Y. F.; Hu, L. G.; Jia, J. P. The co-benefit of elemental mercury oxidation and slip ammonia abatement with SCR-Plus catalysts. *Fuel* **2014**, *133*, 263−269.

(9) Yan, N. Q.; Chen, W. M.; Chen, J.; Qu, Z.; Guo, Y. F.; Yang, S. J.; Jia, J. P. Significance of $RuO_2$ modified SCR catalyst for elemental mercury oxidation in coal-fired flue gas. *Environ. Sci. Technol.* **2011**, *45* (13), 5725−5730.

(10) Karim, A. M.; Prasad, V.; Mpourmpakis, G.; Lonergan, W. W.; Frenkel, A. I.; Chen, J. G.; Vlachos, D. G. Correlating particle size and shape of supported $Ru/\gamma\text{-}Al_2O_3$ catalysts with $NH_3$ decomposition activity. *J. Am. Chem. Soc.* **2009**, *131* (34), 12230−12239.

(11) Wang, Q. Y.; Zhao, B.; Li, G. F.; Zhou, R. X. Application of rare earth modified Zr-based ceria-zirconia solid solution in three-way catalyst for automotive emission control. *Environ. Sci. Technol.* **2010**, *44* (10), 3870−3875.

(12) Ko, J. H.; Park, S. H.; Jeon, J.-K.; Kim, S.-S.; Kim, S. C.; Kim, J. M.; Chang, D.; Park, Y.-K. Low temperature selective catalytic reduction of NO with $NH_3$ over Mn supported on $Ce_{0.65}Zr_{0.35}O_2$ prepared by supercritical method: Effect of Mn precursors on NO reduction. *Catal. Today* **2012**, *185* (1), 290−295.

(13) Zhang, L.; He, H. Mechanism of selective catalytic oxidation of ammonia to nitrogen over $Ag/Al_2O_3$. *J. Catal.* **2009**, *268* (1), 18−25.

(14) van den Broek, A. C. M. *Low Temperature Oxidation of Ammonia Over Platinum and Iridium Catalysts*. Ph.D. Thesis, Technische Universiteit Eindhoven, Eindhoven, 1998.

(15) Yu, T. Y.; Zeng, J.; Lim, B.; Xia, Y. N. Aqueous-phase synthesis of $Pt/CeO_2$ hybrid nanostructures and their catalytic properties. *Adv. Mater.* **2010**, *22* (45), 5188−5192.

(16) Hertl, W. Surface chemistry of zirconia polymorphs. *Langmuir* **1989**, *5* (1), 96−100.

(17) Peng, Y.; Li, J. H.; Chen, L.; Chen, J. H.; Han, J.; Zhang, H.; Han, W. Alkali metal poisoning of a $CeO_2$−$WO_3$ catalyst used in the selective catalytic reduction of NOx with $NH_3$: An experimental and theoretical study. *Environ. Sci. Technol.* **2012**, *46* (5), 2864−2869.

(18) Kamata, H.; Takahashi, K.; Odenbrand, C. I. Surface acid property and its relation to SCR activity of phosphorus added to commercial $V_2O_5$ ($WO_3$)/$TiO_2$ catalyst. *Catal. Lett.* **1998**, *53* (1−2), 65−71.

(19) Chen, L.; Li, J. H.; Ge, M. F. The poisoning effect of alkali metals doping over nano $V_2O_5$−$WO_3/TiO_2$ catalysts on selective catalytic reduction of NOx by $NH_3$. *Chem. Eng. J.* **2011**, *170* (2), 531−537.

(20) Cao, F.; Xiang, J.; Su, S.; Wang, P. Y.; Sun, L. S.; Hu, S.; Lei, S. Y. The activity and characterization of MnOx-$CeO_2$-$ZrO_2/\gamma\text{-}Al_2O_3$ catalysts for low temperature selective catalytic reduction of NO with $NH_3$. *Chem. Eng. J.* **2014**, *243*, 347−354.

(21) Casapu, M.; Krocher, O.; Mehring, M.; Nachtegaal, M.; Borca, C.; Harfouche, M.; Grolimund, D. Characterization of Nb-containing MnOx−$CeO_2$ catalyst for low-temperature selective catalytic reduction of NO with $NH_3$. *J. Phys. Chem. C* **2010**, *114* (21), 9791−9801.

(22) Xu, W. Q.; He, H.; Yu, Y. B. Deactivation of a $Ce/TiO_2$ catalyst by $SO_2$ in the selective catalytic reduction of NO by $NH_3$. *J. Phys. Chem. C* **2009**, *113* (11), 4426−4432.

(23) Sun, D. K.; Liu, Q. Y.; Liu, Z. Y.; Gui, G. Q.; Huang, Z. Adsorption and oxidation of $NH_3$ over $V_2O_5$/AC surface. *Appl. Catal., B: Environ.* **2009**, *92* (3), 462−467.

(24) Wang, X. Q.; Shi, A. J.; Duan, Y. F.; Wang, J.; Shen, M. Q. Catalytic performance and hydrothermal durability of $CeO_2$−$V_2O_5$−$ZrO_2/WO_3$−$TiO_2$ based $NH_3$-SCR catalysts. *Cata. Sci. Technol.* **2012**, *2* (7), 1386−1395.

(25) Liu, Z. M.; Yi, Y.; Li, J. H.; Woo, S. I.; Wang, B. Y.; Cao, X. Z.; Li, Z. X. A superior catalyst with dual redox cycles for the selective reduction of NOx by ammonia. *Chem. Commun.* **2013**, *49* (70), 7726−7728.

(26) Yang, S. J.; Wang, C. Z.; Li, J. H.; Yan, N. Q.; Ma, L.; Chang, H. Z. Low temperature selective catalytic reduction of NO with $NH_3$ over Mn−Fe spinel: Performance, mechanism and kinetic study. *Appl. Catal., B: Environ.* **2011**, *110*, 71−80.

(27) Maeda, N.; Urakawa, A.; Baiker, A. Support effects and chemical gradients along the catalyst bed in NOx storage-reduction studied by space-and time-resolved in situ DRIFTS. *J. Phys. Chem. C* **2009**, *113* (38), 16724−16735.

(28) Sheu, S. P.; Karge, H. G.; Schlögl, R. Characterization of activated states of ruthenium-containing zeolite NaHY. *J. Catal.* **1997**, *168* (2), 278−291.

(29) Liu, F. D.; Asakura, K.; He, H.; Shan, W. P.; Shi, X. Y.; Zhang, C. B. Influence of sulfation on iron titanate catalyst for the selective catalytic reduction of NOx with $NH_3$. *Appl. Catal., B: Environ.* **2011**, *103* (3), 369−377.

(30) Jiang, B. Q.; Wu, Z. B.; Liu, Y.; Lee, S. C.; Ho, W. K. DRIFT study of the $SO_2$ effect on low-temperature SCR reaction over Fe−$Mn/TiO_2$. *J. Phys. Chem. C* **2010**, *114* (11), 4961−4965.

(31) Granite, E. J.; Pennline, H. W. Photochemical removal of mercury from flue gas. *Ind. Eng. Chem. Res.* **2002**, *41* (22), 5470−5476.

(32) Presto, A. A.; Granite, E. J.; Karash, A. Further investigation of the impact of sulfur oxides on mercury capture by activated carbon. *Ind. Eng. Chem. Res.* **2007**, *46* (24), 8273−8276.

(33) Presto, A. A.; Granite, E. J. Impact of sulfur oxides on mercury capture by activated carbon. *Environ. Sci. Technol.* **2007**, *41* (18), 6579−6584.